Geomechanics and Engineering, *Vol. 33, No. 2 (2023) 133-140*
https://doi.org/10.12989/gae.2023.33.2.133

Surface erosion of MICP-treated sands: Erosion function apparatus tests and CFD-DEM bonding model

Soo-Min Ham[1], Min-Kyung Jeon[2] and Tae-Hyuk Kwon*[3]

[1]*Department of Civil and Environmental Engineering, University of California Davis, 1 Shields Ave, Davis, CA 95616, USA*
[2]*CO2 Geological Storage Research Center, Korea Institute of Geoscience and Mineral Resources, 124 Gwahak-ro, Yuseong-gu, Daejeon 34132, Republic of Korea*
[3]*Department of Civil Engineering, Korea Advanced Institute for Science and Technology, 291 Daehak-ro, Yuseong-gu, Daejeon 34141, Republic of Korea*

(*Received November 29, 2022, Revised March 7, 2023, Accepted March 21, 2023*)

Abstract. Soil erosion can cause scouring and failures of underwater structures, therefore, various soil improvement techniques are used to increase the soil erosion resistance. The microbially induced calcium carbonate precipitation (MICP) method is proposed to increase the erosion resistance, however, there are only limited experimental and numerical studies on the use of MICP treatment for improvement of surface erosion resistance. Therefore, this study investigates the improvement in surface erosion resistance of sands by MICP through laboratory experiments and numerical modeling. The surface erosion behaviors of coarse sands with various calcium carbonate contents were first investigated via the erosion function apparatus (EFA). The test results showed that MICP treatment increased the overall erosion resistance, and the contribution of the precipitated calcium carbonate to the erosion resistance and critical shear stress was quantified in relation to the calcium carbonate contents. Further, these surface erosion processes occurring in the EFA test were simulated through the coupled computational fluid dynamics (CFD) and discrete element method (DEM) with the cohesion bonding model to reflect the mineral precipitation effect. The simulation results were compared with the experimental results, and the developed CFD-DEM model with the cohesion bonding model well predicted the critical shear stress of MICP-treated sand. This work demonstrates that the MICP treatment is effective in improving soil erosion resistance, and the coupled CFD-DEM with a bonding model is a useful and promising tool to analyze the soil erosion behavior for MICP-treated sand at a particle scale.

Keywords: CFD-DEM; cohesion bonding model; EFA; erosion resistance; MICP; soil erosion

1. Introduction

Erosion of soils is a ubiquitous phenomenon that often leads to scouring and failures of underwater geo-structures by reducing the ground bearing capacity and geometric confinement around structures (Prendergast and Gavin 2014). Identification of the erosion characteristics and resistance of soils is important to predict soil erosion and scour for design of underwater structures (Briaud *et al.* 1999, 2001, De Falco and Mele 2002, Jacobs *et al.* 2011, Prendergast and Gavin 2014). Soil erosion occurs once shear stress exerted by moving fluids exceeds a critical value, referred to as the critical shear stress (Jacobs *et al.* 2011). And the erodibility coefficient indicates the sensitivity of the erosion rate against shear stress increment, which means how fast the erosion rate increases when the soil is subjected to an increase in shear stress. Accordingly, the lab-scale experimental studies have investigated the critical shear stress and erodibility coefficient of various soils (Arulanandan and Perry 1983, Hanson and Cook 2004, Wan and Fell 2004, Kwon *et al.* 2021).

Mitigating the erosion in underwater soils is thus critical to ensure the stability of soil structures such as dams, embankments, levees, and bridge foundations (Melville and Coleman 2000; De Falco and Mele 2002). To increase the soil erosion resistance, various ground improvement techniques have been used, including chemical grouting (Basha *et al.* 2005, Chhun *et al.* 2020), piling (Chiew 1992, Heidarpour *et al.* 2010), and erosion control blanket (Vick 1984, Ahn *et al.* 2002).

Microbially induced calcium carbonate precipitation (MICP) has recently gained attention as an environment-friendly ground improvement method (Yu 2021). This method exploits the precipitation of calcium carbonate minerals as a result of bacterial metabolic activity. Microorganisms hydrolyze and decompose urea into carbonate ions (CO_3^{2-}) by using enzyme called urease. When calcium ion (Ca^{2+}) is introduced, solid calcium carbonate ($CaCO_3$) crystals are precipitated due to its low solubility. The produced calcium carbonate minerals act as a cementation agent to bond soil particles, and improve the engineering properties while its extent of improvement depends on the amount of calcium carbonate precipitated.

This MICP treatment has been proposed proven for the erosion control against internal erosion as it contributes to enhancement in the critical shear stress and reduction in the erosion coefficient through the inter-particle cementation (Bang *et al.* 2011, Jiang *et al.* 2017, Montoya *et al.* 2018,

*Corresponding author, Associate Professor
E-mail: t.kwon@kaist.ac.kr

ISSN: 2005-307X (Print), 2092-6219 (Online)

Do *et al.* 2019, He *et al.* 2021). Whereas, the use of MICP treatment for control of surface erosion is still limited.

Therefore, this study investigates the improvement in surface erosion resistance of sands by MICP through laboratory experiments and numerical modeling. The surface erosion rates of coarse sands with various calcium carbonate contents (or *CC*) were measured with the erosion function apparatus (EFA) developed by Briaud *et al.* (1999, 2001). The contribution of the calcium carbonate (or calcite) to the erosion resistance and critical shear stress was quantified in relation to *CC*. And the erosion behavior of MICP treated sand was simulated by using numerical model coupling computational fluid dynamics (CFD) and discrete element method (DEM) with a cohesion bonding model to study soil erosion mechanisms at a particle scale.

2. Experimental program

2.1 Biological treatment

Sporosarcina pasteurii (American Type Culture Collection, ATCC 11859) was used as the model bacterium for MICP treatment in this study, owing to its high urease activity (DeJong *et al.* 2022). For culturing the model bacteria, ammonium-yeast extract media (growth media; ATCC 1376) was used, which contained 20 g/L yeast extract, 10 g/L ammonium sulfate ($(NH_4)_2SO_4$), and 0.13 M Tris buffer (pH = 9.0). Individual components were autoclaved separately at 121°C for 15 min, and mixed together. The model bacteria *S. pasteurii* were aerobically cultured in the growth medium at 30°C in shaking incubator at 200 rpm for 20 hours to achieve an optical density (OD_{600}) of 1.0. The bacterial culture was centrifuged at 4000 g for 40 min, and then the supernatant was discarded and replaced with the fresh growth media. This was then stored in the refrigerator at 4°C prior to use, and later was used as a bacterial inoculum.

The cementation solution contained 350 mM of urea ($CO(NH_2)_2$) for ureolysis, 350 mM of calcium chloride ($CaCl_2$) as a calcium source, 2 g/L of yeast extract as nutrients, 250 mM of ammonium chloride (NH_4Cl), and 42.5 mM of sodium acetate ($C_2H_3NaO_2$), and this was used to stimulate ureolysis and calcite precipitation.

2.2 Sample preparation

Coarse sand (Ottawa 20/30, U.S. Silica, Frederick, MD, USA) was used as the host soil. Fig. 1 shows the particle shape, particle size distribution, and basic index properties of the tested sand. The sand had a uniform size distribution with a mean diameter of 0.77 mm, and the particles were fairly round and spherical.

The sand specimens for EFA tests were prepared by air-pluviation in a thin-wall tube with an internal diameter of 69 mm and a height of 200 mm. This study used a two-phase injection method, where the bacterial cell solution was first inoculated, followed by the cementation solution injection (Whiffen *et al*. 2007). Fig. 2 shows the MICP treatment configuration.

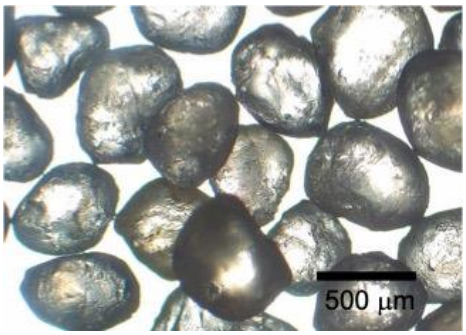

(a)

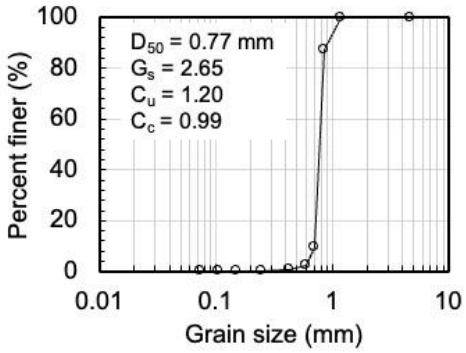

(b)

Fig. 1 (a) An optical microscope image and (b) particle size distribution curve of the tested sand. D_{50} is the mean grain size, G_S is the specific gravity of mineral, C_u is the coefficient of uniformity, and C_c is the coefficient of curvature

Initially, the bacterial inoculum containing the model bacteria *S. pasteurii* was injected into the sand column for three pore volumes, and the bacteria were then retained for 24 hours under no mass flux for bacterial attachment to sand grains. The column was then flushed with the fixation solution for two pore volumes. The fixation solution contained only 9 g/L of sodium chloride (NaCl) in de-ionized water, and its high ionic concentration is reported to facilitate attachment of bacteria on solid surfaces and homogeneous distribution within a sand specimen (Harkes *et al*. 2010). In addition, the flushing process displaced the excessive and suspended bacteria and sulfate ion which minimized formation of gypsum ($CaSO_4$). The cementation solution was introduced into the column for two pore volumes, and the retention time of 24 hours was given for sufficient reaction process. After the retention time, this cementation treatment was repeated. Upon two treatments with the cementation solution, the specimen was flushed with the ammonium chloride solution to avoid the reaction between the remaining calcium ions and sulfate in the bacteria inoculum. Then, another cycle resumed again from the bioaugmentation with bacterial inoculum. The cycles were repeated until the specimen reached the target calcite content (*CC*). The weight of the specimen and urea concentration of the effluent were monitored during the injection. The flow rate for all injection processes was set to 15 mL/min.

The calcite content (*CC*) is defined as the weight of calcium carbonate precipitated divided by the weight of dry

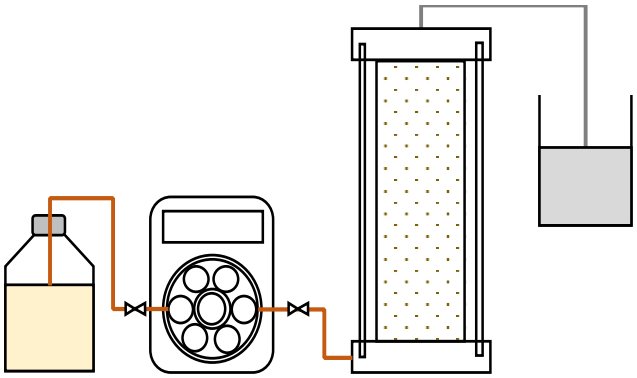

Fig. 2 Experiment setup for MICP treatment

soil, which indicates the amount of calcite precipitated and the level of cementation. In this study, three specimens were prepared at various *CC* levels: the reference specimen without any treatment (*CC* = 0%), specimen with *CC* = 2.4%, and specimen with *CC* = 4.6%. Hereafter, the specimens are referred with the *CC* level: CC0 for 0%, CC2 for 2.4%, and CC4 for 4.6%. The description of soil specimens is summarized in Table 1.

2.3 Erosion function apparatus (EFA) test

The erosion function apparatus (EFA) developed by Briaud *et al*. (1999, 2001) was used to investigate the surface erosion behavior of the MICP-treated sands. This test is widely used to estimate the erosion rate of fine- and coarse-grained soils. The EFA test was conducted, following the suggested procedure by Briaud *et al*. (1999).

A thin-walled tube with MICP-treated sand was placed at the bottom of the water flow channel. Once the water flow rate was set and stabilized, a 1-mm-thick soil protrusion was exposed to the water flow by pushing the bottom of the specimen. This soil protrusion was eroded by the shear force exerted by the water flow. The erosion time, defined as the time taken to erode the 1-mm-thick soil protrusion, was measured, and the erosion rate was calculated by dividing the eroded soil depth (i.e., 1 mm) by the erosion time taken. The shear stress (τ_{fluid}) acting on the soil surface can be calculated, as follows:

$$\tau_{fluid} = \frac{1}{8} f \rho_{fluid} v^2, \quad (1)$$

where f is the friction factor and can be obtained from Moody's chart (Moody 1944), ρ_{fluid} is the density of water, and v is the mean flow velocity. The erosion rate was obtained at various flow velocities and plotted against the corresponding shear stress to produce the erosion curve. A P-wave monitoring system developed by Ham *et al*. (2016) was implemented in the EFA to provide more accurate measurement. Three pairs of ultrasonic sensors were mounted at the top of the fluid channel, and named as Channels 1, 2, and 3; Ch1 monitored the soil depth at the front region, Ch2 was at the middle region, and Ch3 was at the back region of a circular surface, respectively. More details of the system are described in Ham *et al.* (2016).

Table 1 Description of soil specimen condition

Symbol	Host grain	Void ratio (-)	Calcite content (%)
CC0	Ottawa 20/30	0.60	0
CC2		0.50	2.39
CC4		0.50	4.57

3. Experimental results

3.1 Erosion behavior of MICP-treated sand

The water velocity increased from 0.17 m/s to 0.35 m/s for CC0, 0.22 m/s to 0.37 m/s for CC2, and 0.27 m/s to 0.35 m/s for CC4, respectively. Fig. 3 shows changes in the soil protrusion depth at three locations on a soil surface at a similar fluid velocity of ~0.35 m/s. Channels 1, 2, and 3 indicate the location of the soil surface along the direction of water flow. For Specimen CC0, the front part was not eroded for 10 seconds (Ch1), while the middle and back parts (Chs 2 and 3) were eroded by 1 mm within 5 seconds (Fig. 3(a)). It implies that this Specimen CC0 without any treatment was the most vulnerable to erosion. For Specimen CC2, the front- and back-sides were not eroded, while the middle region was eroded very fast (Fig. 3(b)). This indicates a highly heterogeneous erosion process due to various cementation levels within a specimen. For Specimen CC4, the specimen was fairly homogeneously eroded, and it takes 10 seconds to erode ~1 mm thick (Fig. 3(c)). Peculiarly, it was noted that the soil depth often increased as captured by Ch3 in Fig. 3(c). This was because the eroded soil from the front was deposited at the back, resulting in the elevation of the soil height.

The EFA method defined the erosion time as the duration taken to erode away a 1-mm-thick soil protrusion that was protruding from the bottom level toward a water flow. The erosion rate was calculated by dividing the erosion depth (i.e., 1 mm here) by the erosion time. In our study, the erosion time for each channel (or each location) was determined by picking the elapsed time until the soil surface was lowered by 1 mm, as indicated by the arrows in Fig. 3(a). Then, the erosion rate ($\dot{z}$) was calculated by dividing 1 mm by the averaged erosion times for all available channels. The signals showing no erosion were excluded from the average. Finally, the erosion rate ($\dot{z}$) versus shear stress curve, or erosion curve, was obtained, as shown in Fig. 3(d).

Specimen CC0 showed the least erosion resistance while Specimen CC4 presented the greatest erosion resistance. Therefore, it is confirmed that the soil with the more calcite precipitation and the higher cementation level showed the greater erosion resistance. The critical shear stress for each specimen was estimated from the erosion curve by following the procedure proposed by Briaud *et al*. (2001). As the more calcite was precipitated, the greater critical shear stress that was observed, e.g., τ_c = 0.1 Pa for CC0, τ_c = 0.16 Pa for CC2, and τ_c = 0.26 Pa for CC4, respectively.

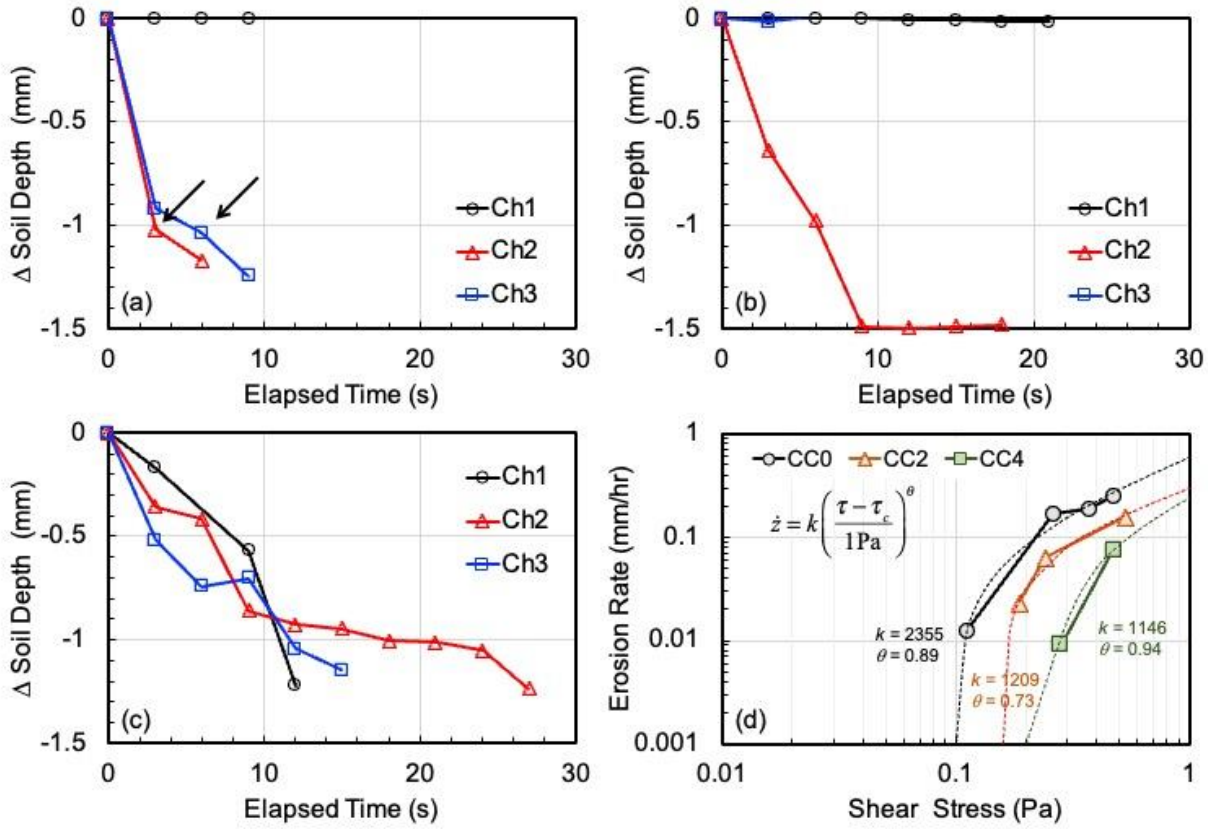

Fig. 3 Changes in the soil depth: (a) CC0 at v = 0.35 m/s, (b) CC2 at v = 0.37 m/s, and (c) CC4 at v = 0.35 m/s, and (d) the erosion curves for all specimens

3.2 Effect of MICP on erosion resistance

The erosion resistance of soils can be described with the power relation between the erosion rate and the excess shear stress (τ-τ_c), as follows (Partheniades 1965, Hanson and Cook 1997, Ham *et al*. 2018)

$$\dot{z} = k\left(\frac{\tau - \tau_c}{1\text{Pa}}\right)^{\theta}, \quad (2)$$

where $\dot{z}$ is the erosion rate (mm/h), τ is the shear stress, τ_c is the critical shear stress (i.e., the minimum shear stress at which soil erosion begins to occur), k is the erodibility coefficient (mm/h), and θ is the power exponent. These erosion resistance parameters indicate how fast the erosion rate increases when the soil is subjected to an increase in shear stress, or the sensitivity of the erosion rate $\dot{z}$ to the difference between the applied shear stress and excess shear stress. The higher k and θ and the lower τ_c imply that the soil is more prone to erosion. Both k and θ decrease and τ_c increases as the soil becomes mechanically strengthened.

Table 2 summarizes the critical shear stress τ_c and the erosion resistance parameters k and θ obtained in this study, and compares with the data reported by Ham *et al.* (2016, 2018). Note that Ham *et al.* (2018) performed the EFA tests on sands treated by microbially induced biopolymer formation with *Leuconostoc mesenteroides*. Ham *et al.* (2018) controlled the sucrose concentration to vary the amount of biopolymer formation; reference case (REF) without bacteria, low biopolymer formation case (S150) with a sucrose concentration of 150 g/L, and high biopolymer formation case (S300) with a sucrose concentration of 300 g/L, respectively. Ham *et al.* (2016) also carried out the EFA tests on sand-kaolinite mixtures with various sand/kaolinite mass ratios of 10:0, 9:1, 8:2, and 7:3 (i.e., S10K0, S9K1, S8K2, and S7K3, respectively).

As expected, the precipitated calcite from MICP treatment caused an increase in the erosion resistance as well as the critical shear stress. As the cementation level increased with *CC*, the critical shear stress significantly increased with only 4% *CC*, e.g., τ_c = 0.1 Pa for CC0, τ_c = 0.16 Pa for CC2, and τ_c = 0.26 Pa for CC4 (see Table 2). In previous studies by Ham *et al.* (2016, 2018), the more biopolymer formation or the higher clay fraction also resulted in the increased critical shear stress. Furthermore, previous studies by Ham *et al.* (2016, 2018) showed that both k and θ parameters decreased with increasing biopolymer formation and clay fraction, as shown in Table 2. In MICP-treated sands, the same tendency of decreasing erosion resistance parameters was confirmed with an increase in *CC*. The erodibility coefficient k decreased from 2355 mm/hr for CC0 to 1146 mm/hr for CC4 and the power exponent θ decreased from 0.89 for CC0 to 0.73 for CC2, respectively. The increased power exponent θ in Specimen CC4 is somewhat ambiguous due to the lack of data points used for the fitting. Conclusively, the results clearly showed that the precipitated calcite improved the erosion resistance, and the extent increased with the cementation level or *CC*.

Table 2 Correlations between critical shear stress and inclusion content

	τ_c (Pa)	k (mm/hr)	θ (-)
MICP (this study)			
CC0	0.1	2355	0.89
CC2	0.16	1209	0.73
CC4	0.26	1146	0.94
Biopolymer Ham *et al*. (2018)			
REF	0.1	9132	1.83
S150	0.19	1657	1.13
S300	0.23	1110	0.88
Sand-kaolinite mixture Ham *et al.* (2016)			
S10K0	0.07	5382	1.07
S9K1	0.18	859	0.75
S8K2	0.18	860	0.53
S7K3	0.2	40	0.56

4. Numerical modeling with coupled CFD-DEM

4.1 Cohesion bonding model for MICP treatment

Cementation due to MICP treatment was described by using the simplified Johnson-Kendall-Roberts bonding model (SJKR, Barthel 2008), which is one of the cohesion bonding models. In addition to the Hertzian contact forces, this model adds an additional normal force (F_{SJKR}) to the particles in contact, as follows

$$F_{SJKR} = \chi A_c \tag{3}$$

where A_c is the particle contact area (m^2) and χ is the cohesion energy density (J/m^3).

The cohesion energy density χ was calibrated based on the experiment results from Ham *et al.* (2022). According to Ham *et al*. (2022), the dominant failure mode evolves with the *CC* level, and the tensile strength is estimated as ~35 kPa when *CC* < 17% and ~8 kPa for *CC* > 17%, respectively. Also, the contact radius can be determined based on the calcite precipitation pattern. The precipitation pattern changes with *CC*: grain-coating mode (*CC* < 15%), meniscus-filling mode (15% < *CC* < 25%), and flat torus-filling mode (*CC* > 20%) models.

For a given *CC* level, the contact radius and contact area can be estimated based on the grain-coating model, and the maximum tensile force between two particles can be calculated by multiplying the contact area with the tensile strength. This maximum tensile force is assumed to be the normal force from SJKR model (F_{SJKR}) to be added as a particle-level force. The normal force from SJKR model

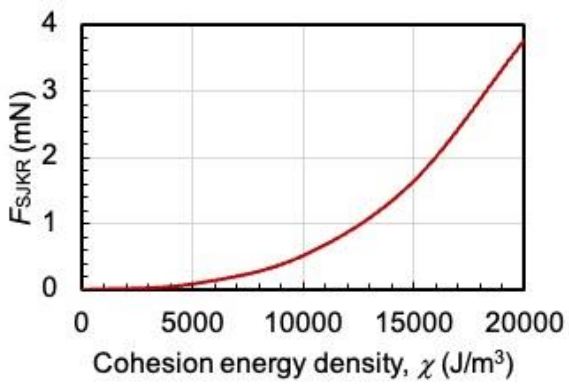

Fig. 4 A correlation between the cohesion energy density and the normal force in SJKR model

(F_{SJKR}) is correlated to the cohesion energy density, as shown in Fig. 4. Accordingly, the corresponding cohesion energy density for a given *CC* level can be calculated.

In this study, the specimen with *CC* = 4.6% was modeled (Specimen CC4). As *CC* was lower than 17%, the tensile strength was 35 kPa and the precipitation pattern followed the grain-coating model, which resulted in the contact area of 0.014 mm^2. Therefore, the maximum tensile force applied on the particles was 0.49 mN with the cohesion energy density of 9,500 J/m^3 with 1.7 μm of overlap.

4.2 Coupled CFD-DEM modeling of surface erosion

The simulation model was constructed by following the actual EFA test setup (Briaud *et al.* 2001). The computational fluid dynamics (CFD) was employed to simulate the water flow and the discrete element method (DEM) was adopted to describe the particle motions. For CFD setting, a rectangular flow channel was generated with a dimension of 1400 × 50 × 50 mm^3 for length (x-direction), width (y-direction), and height (z-direction), respectively. The water flowed in and out through the inlet and outlet of this channel, and the k-ω turbulent flow model was used to describe the turbulency. The inlet velocity varied from 0.20 to 0.47 m/s, and to 0.47 m/s for comparison with the experimental results. For DEM setup, a cylindrical specimen with a diameter of 10 mm was modeled, in which the particles had the same particle size distribution with the tested sand (Fig. 1). The sand specimen was prepared by following these steps: (a) the particles were generated in the box above the soil tube, (b) the generated particles were pluviated and then packed in the tube with a cohesion value, (c) the particles outside of the soil tube were removed, and (d) the particles were pushed up for 1-mm thick protrusion. This particle pack specimen was located at the bottom of the flow channel, 1300 mm away from the inlet along the flow direction (x-direction). A total of 514 particles were used. Then, the coupled CFD-DEM analysis was performed to simulate the EFA test. The DEM time step was set as 10^{-6} s and the CFD time step was set as 10^{-4} s with the coupling interval of 100. The total simulation time was 3 s. For the first 1 s, the

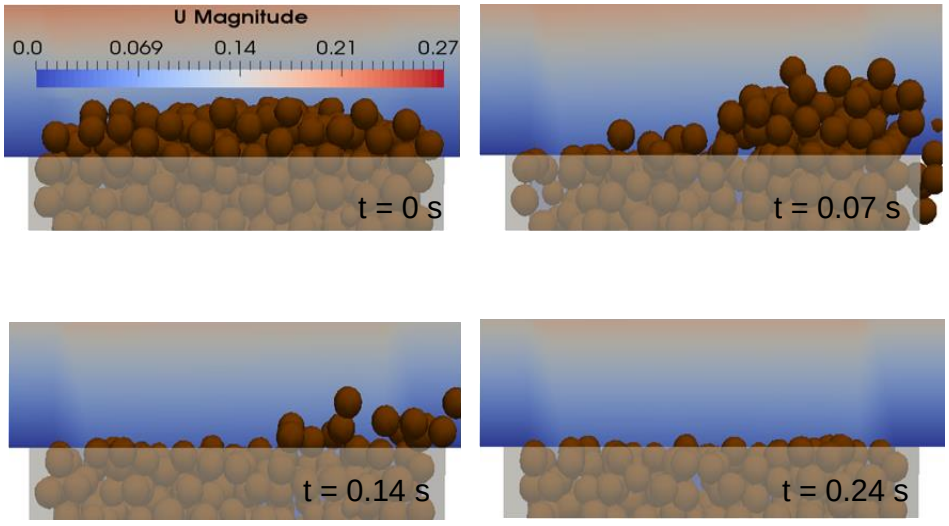

(a)

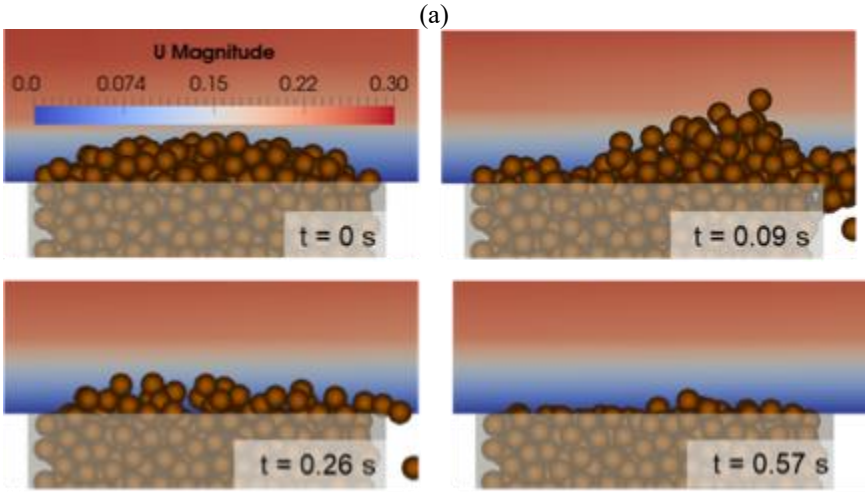

(b)

Fig. 5 Snapshots for the particle erosion process: (a) untreated specimen (CC0) at v = 0.26 m/s and (b) MICP-treated specimen (CC4) at v = 0.27 m/s

particle location was fixed until the fluid flowed at a steady state, and thereafter, the erosion process was simulated for the next 2 s. The Di Felice drag force (Di Felice 1994), pressure gradient force, viscous force, and buoyancy force were calculated and taken into account as the particle-fluid interaction forces. Three cases for Specimen CC0 and two cases for Specimen CC4 were simulated while varying the water velocity.

5. Simulation results and discussion

5.1 Particle erosion behavior and critical shear stress

The simulation results depicted the surface erosion of soil particles due to the shear stress applied by a water flow. Fig. 5 shows the particle-level erosion processes of untreated and MICP-treated sands at the water velocity v of 0.26–0.27 m/s. It appears that the water flow velocity was lower near the soil specimen than the average flow velocity, and the soil particles moved along the flow direction. Soil erosion continued until the force induced by the water flow was insufficient to erode the particles. While continuous erosion occurred from the back-side to the front-side of the specimen was observed in the untreated specimen (Fig. 5(a)), the MICP-treated specimen was eroded in a heterogeneous way (Fig. 5(b)).

The erosion rate was estimated by analyzing the change in soil protrusion depth, and the erosion curve was obtained as Fig. 6. The MICP-treated sands showed the higher critical shear stress and erosion resistance, which was consistent with the experimental results. The erosion curves obtained from the experiment were superimposed in Fig. 6.

It was found that the coupled CFD-DEM analysis with cohesion bonding model well captured the critical shear stress. However, the simulation overestimated the erosion rates. At a particle scale in MICP-treated sands, even though the bulk calcite content is 4%, the cementation level at individual contacts shows a fairly wide distribution (Ham *et al.* 2022). As a result, the cementation may show a progressive failure with time for a given flow velocity in the actual erosion tests. By contrast, our study assumed the uniform *CC* level and thus uniform bonding force between

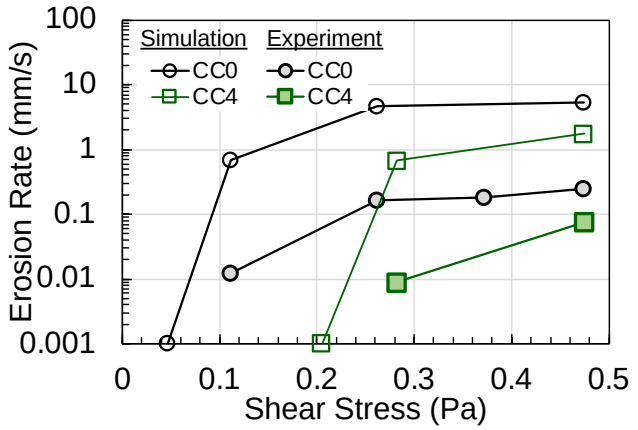

Fig. 6 Erosion curves of CC0 and CC4 specimens from the coupled CFD-DEM analysis and experiments

contacts in the DEM modeling. Thus, majority of the particle bonds was broken simultaneously in the simulations, and after bonding breakage, the erodibility was hardly affected whether it was treated by MICP or not.

5.2 Implication and limitation

The simulation results suggest that the cohesion bonding model properly captures the effect of MICP-treatment on the critical shear stress τ_c as the normal force from SJKR bonding model provides additional resistance against the shear force. Meanwhile, it is found that the simulation has limitation in estimating the erosion coefficients k and θ of MICP-treated sand. This limitation is attributable to two reasons: the increased angularity and roughness of MICP-treated grains, and a grain-scale variation in cementation level among contacts. The erosion resistance can be affected by the increased particle angularity and surface roughness by MICP. Meanwhile, the bulk densification through the void fillings is expected to be minimal for a low cementation level, e.g., $CC < 5\%$. The presented CFD-DEM modeling assumes a uniform cementation level with a uniform tensile strength value within a specimen. However, the cementation level inevitably varies with grain sizes and there is always some level of heterogeneity in cementation even at a specimen scale. Therefore, such a variation in cementation level would cause a progressive failure in particle bonding by flow-driven shear forces, which is required to be taken into account in DEM modeling. Moreover, the relationship between the cohesion energy density and additional normal force is also presumed to change whieh varying particle characteristics. Therefore, further research is needed with different CC levels, their distributions, soil types, particle size, and void ratio.

5. Conclusions

This study investigated the improvement of surface erosion resistance of MICP-treated sand through the experimental study and coupled CFD-DEM analysis with cohesion bonding model. The major findings are as follows:

- The MICP treatment increased the overall erosion resistance, including the critical shear stress. An increase in CC increased the critical shear stress and the erosion resistance.
- The erosion rates of MICP-treated sands were correlated to the excess shear stress with two erosion resistance parameters, the erodibility coefficient k and power exponent θ. The both parameters were observed to decrease with the increasing CC.
- The comparative study with the physical experiments revealed that the developed coupled CFD-DEM model with a cohesion bonding model was capable of prediction of the critical shear stress for MICP-treated sands.

The presented work suggests that the MICP treatment is effective in improving surface erosion resistance of sands, and at the same time, the coupled CFD-DEM with a bonding model is a useful tool to predict the soil erosion behavior for MICP-treated sands.

Acknowledgments

This paper was supported by "Ministry of the Interior and Safety" R&D program (20018265), and also supported by the Korea Electric Power Corporation (Grant R22XO05-11).

References

Ahn, T., Cho, S. and Yang, S. (2002), "Stabilization of soil slope using geosynthetic mulching mat", *Geotext. Geomembranes*, **20**(2), 135-146. https://doi.org/10.1016/S0266-1144(02)00002-X.

Arulanandan, K. and Perry, E. (1983), "Erosion in relation to filter design criteria in Earth Dams", *J. Geotech. Eng.*, **109**(5), 682-698. https://doi.org/10.1061/(ASCE)0733-9410(1983)109:5(682).

Bang, S., Min, S. and Bang, S. (2011), "Application of microbiologically induced soil stabilization technique for dust suppression", *Int. J. Geo-Eng.*, **3**(2), 27-37.

Barthel, E. (2008), "Adhesive elastic contacts: JKR and more", *J. Phys. D: Appl. Phys.*, **41**(16), 163001. 10.1088/0022-3727/41/16/163001.

Basha, E., Hashim, R., Mahmud, H. and Muntohar, A. (2005), "Stabilization of residual soil with rice husk ash and cement", *Constr. Build. Mater.*, **19**(6), 448-453. https://doi.org/10.1016/j.conbuildmat.2004.08.001.

Briaud, J., Ting, F., Chen, H., Cao, Y., Han, S. and Kwak, K. (2001), "Erosion function apparatus for scour rate predictions", *J. Geotech. Geoenviron. Eng.*, **127**(2), 105-113. https://doi.org/10.1061/(ASCE)1090-0241(2001)127:2(105).

Briaud, J., Ting, F., Chen, H., Gudavalli, R., Perugu, S. and Wei, G. (1999), "SRICOS: Prediction of scour rate in cohesive soils at bridge piers", *J. Geotech. Geoenviron. Eng.*, **125**(4), 237-246. https://doi.org/10.1061/(ASCE)1090-0241(1999)125:4(237).

Chhun, K.T., Choo, H., Kaothon, P. and Yune, C.Y. (2020), "Experimental study on the strength behavior of cement-stabilized sand with recovered carbon black", *Geomech. Eng.*, **23**(1), 31-38. https://doi.org/10.12989/gae.2020.23.1.031.

Chiew, Y. (1992), "Scour protection at bridge piers", *J. Hydraulic Eng.*, **118**(9), 1260-1269. https://doi.org/10.1061/(ASCE)0733-

9429(1992)118:9(1260).
De Falco, F. and Mele, R. (2002), "The monitoring of bridges for scour by sonar and sedimetri", *NDT & E Int*., **35**(2), 117-123. https://doi.org/10.1016/S0963-8695(01)00031-7.
DeJong, J.T., Gomez, M.G., San Pablo, A.C., Graddy, C.M.R., Nelson, D.C., Lee, M., Ziotopoulou, K., El Kortbawi, M., Montoya, B. and Kwon, T.H. (2022), "State of the Art: MICP soil improvement and its application to liquefaction hazard mitigation", *Proceedings of the 20th ICSMGE-State of the Art and Invited Lectures*, Sydney, Australia, May.
Di Felice, R. (1994), "The voidage function for fluid-particle interaction systems", *Int. J. Multiphase Flow*, **20**(1), 153-159. https://doi.org/10.1016/0301-9322(94)90011-6.
Do, J., Montoya, B.M. and Gabr, M.A. (2019), "Debonding of microbially induced carbonate precipitation-stabilized sand by shearing and erosion", *Geomech. Eng.*, **17**(5), 429-438. https://doi.org/10.12989/gae.2019.17.5.429.
Ham, S.M., Chang, I., Noh, D.H., Kwon, T.H. and Muhunthan, B. (2018), "Improvement of surface erosion resistance of sand by microbial biopolymer formation", *J. Geotech. Geoenviron. Eng.*, **144**(7), 06018004. https://doi.org/10.1061/(ASCE)GT.1943-5606.0001900.
Ham, S.M., Kwon, T.H., Chang, I. and Chung, M.K. (2016) "Ultrasonic p-wave reflection monitoring of soil erosion for erosion function apparatus", *Geotech. Test. J.*, **39**(2), 301-314. https://doi.org/10.1520/GTJ20150040.
Ham, S.M., Martinez, A., Han, G. and Kwon, T.H. (2022), "Grain-scale tensile and shear strengths of glass beads cemented by MICP", *J. Geotech. Geoenviron. Eng.*, **148**(9), 04022068. https://doi.org/10.1061/(ASCE)GT.1943-5606.0002863.
Hanson, G.J. and Cook, K.R. (2004), "Apparatus, test procedures, and analytical methods to measure soil erodibility in situ", *Appl. Eng. Agriculture*, **20**(4), 455-462. https://doi.org/10.13031/2013.16492.
Harkes, M., Van Paassen, L., Booster, J., Whiffin, V. and van Loosdrecht, M. (2010), "Fixation and distribution of bacterial activity in sand to induce carbonate precipitation for ground reinforcement", *Ecol. Eng.*, **36**(2), 112-117. https://doi.org/10.1016/j.ecoleng.2009.01.004.
He, J., Fang, C., Hang, L., Qi, Y., Mao, X., Yan, B., Zhou , Y. and Gao, Y. (2021), "Enzyme induced carbonate precipitation for soil internal erosion control under water seepage", *Geomech. Eng.*, **26**(3), 289-299. https://doi.org/10.12989/gae.2021.26.3.289.
Heidarpour, M., Afzalimehr, H. and Izadinia, E. (2010), "Reduction of local scour around bridge pier groups using collars", *Int. J. Sediment Res.*, **25**(4), 411-422. https://doi.org/10.1016/S1001-6279(11)60008-5.
Jacobs, W., Le Hir, P., Van Kesteren, W. and Cann, P. (2011), "Erosion threshold of sand–mud mixtures", *Continental Shelf Res.*, **31**(10), S14-S25. https://doi.org/10.1016/j.csr.2010.05.012.
Jiang, N. and Soga, K. (2017), "The applicability of microbially induced calcite precipitation (MICP) for internal erosion control in gravel–sand mixtures", *Géotechnique*, **67**(1), 42-55. https://doi.org/10.1680/jgeot.15.P.182.
Kwon, Y.M., Cho, G.C., Chung, M.K. and Chang, I. (2021), "Surface erosion behavior of biopolymer-treated river sand", *Geomech. Eng.*, **25**(1), 49-58. https://doi.org/10.12989/gae.2021.25.1.049.
Melville, B. and Coleman, S. (2000), *Bridge Scour*, Water Resources Publication, Colorado, USA.
Montoya, B.M., Do, J. and Gabr, M.M. (2018), "Erodibility of microbial induced carbonate precipitation-stabilized sand under submerged impinging jet", *Proceedings of the International Foundation Congress and Equipment Expo*, Orlando, Florida, USA, March. https://doi.org/10.1061/9780784481592.003.
Moody, L.F. (1944), "Friction factors for pipe flow", *Transactions of the American Society of Mechanical Engineers*, **66**(8), 671-684.
Prendergast, L.J. and Gavin, K. (2014), "A review of bridge scour monitoring techniques", *J. Rock Mech. Geotech. Eng.*, **6**(2), 138-149. https://doi.org/10.1016/j.jrmge.2014.01.007.
Vick, D. (1984), "Concrete revetment mat systems for Shore erosion control on offshore embankments", *Proceedings of the Annual Offshore Technology Conference*, Houston, Texas, USA, May. https://doi.org/10.4043/4673-MS.
Wan, C. and Fell, R. (2004), "Laboratory tests on the rate of piping erosion of soils in embankment dams", *Geotech. Test. J.*, **27**(3), 295-303. https://doi.org/10.1520/GTJ11903.
Whiffin, V., van Paassen, L. and Harkes, M. (2007), "Microbial carbonate precipitation as a soil improvement technique", *Geomicrobiol. J.*, **24**(5), 417-423. https://doi.org/10.1080/01490450701436505.
Yu, T. (2021), "Review on engineering properties of MICP-treated soils", *Geomech. Eng.*, **27**(1), 13-30. https://doi.org/10.12989/gae.2021.27.1.013.